

Latent Photoinduced Oxygen Doping Revealed from Emission Saturation of Aggregated Domains in Conjugated Polymer Nanofibers

David J. Walwark Jr., Thomas P. Martin Jr., and John K. Grey*

Photoinduced oxidation (doping) of conjugated polymers by complexation with oxygen can have a significant impact on electronic properties and performance in device environments. Nanofiber model forms of poly(3-hexylthiophene) (P3HT) are investigated using single molecule spectroscopy that possess similar morphological qualities as their bulk thin film counterparts yet, heterogeneity is confined to the spatial dimensions of these particles. Specifically, P3HT nanofibers assembled in anisole solutions contain both aggregated and nonaggregated (amorphous) chains with distinct electronic properties. Excitation intensity dependent photoluminescence (PL) emission imaging is then used to expose differences in oxygen affinity and reactivity upon photoexcitation. Nanofiber regions with low PL yields tend to show faster PL intensity saturation that also degrade much faster following periods of high excitation intensity soaking. Conversely, other regions show gains in PL intensity and virtually no saturation. These PL “gainer” and “loser” behaviors are assigned as originating from amorphous and aggregated P3HT chains, respectively. The apparent propensity of aggregated chains to undergo latent oxygen doping indicates a greater affinity probably due to a larger extent of electronic delocalization in these structures. The results shed new light on degradation factors studied frequently at the bulk material level, which often lacks sufficient sensitivity to specific structural forms.

1. Introduction

Minority impurities can profoundly impact the electronic properties of conjugated polymers for optoelectronic devices even when rigorous precautions are taken during processing. Among the most detrimental to performance and long-term material stability is doping by oxygen, which is greatly accelerated in the presence of light but may also occur more slowly


in the dark.^[1,2] Understanding the basic nature of polymer–oxygen interactions has received considerable attention from both fundamental and applied (device) perspectives.^[1,3] A wide range of spectroscopic and electrochemical probes have been leveraged to resolve how oxygen interacts with polymer chains in either solution or solid phase forms. However, heterogeneity effects originating from molecular weight polydispersity and large conformational degrees of freedom usually mask molecular details by ensemble averaging of thin films. The fact that many polymers also exist in distinct structural forms (i.e., conformers or polymorphs of crystalline aggregates) with different electronic properties further complicates this understanding since interactions and reactivities with oxygen should depend on structural qualities.

Despite that oxygen doping affects nearly all conjugated organic polymers, many studies have focused on poly(3-hexylthiophene) (P3HT), which has seen extensive use in various device applications.^[4] P3HT also readily assembles into

semicrystalline, π -stacked aggregated domains with markedly different electronic properties than nonaggregated, solvated chains.^[5] Interestingly, evidence of preferential interactions between oxygen and P3HT forms has been inferred from comparisons of samples with different regioregularity. For example, P3HT chains of high regioregularity have large aggregate content in thin solid films as opposed to regiorandom variants that exist primarily in solution-like (nonaggregated) conformations. Photostability studies of P3HT thin films in air using ensemble absorption spectroscopy found that aggregates tend to bleach faster than solvated-type chromophores.^[6,7] This effect can be attributed to the greater extent of electronic delocalization (i.e., intra- and interchain directions) in aggregates leading to lower oxidation potentials.^[8,9] Furthermore, a shift of 0.2 V in the oxidation potential from annealing-induced crystallization has also been found.^[10] It is also noteworthy energy differences between both forms are greater than 0.18 eV corresponding to a 1000× difference in Boltzmann occupancies. Similar trends have been reported in studies of charge transfer doping where greater regioregularity and higher aggregate content are correlated with higher doping efficiencies.^[11] The broad tunability

D. J. Walwark Jr., Prof. J. K. Grey
Department of Chemistry and Chemical Biology
University of New Mexico
Albuquerque, NM 87131, USA
E-mail: jkgrey@unm.edu

Dr. T. P. Martin Jr.
Department of Chemistry
University of Wyoming
Laramie, WY 82071, USA

 The ORCID identification number(s) for the author(s) of this article can be found under <https://doi.org/10.1002/aelm.202000265>.

DOI: 10.1002/aelm.202000265

and variability of both aggregate content and crystallinity with material processing conditions, however, make pinning down specific oxygen doping products with polymer forms difficult. Currently, very little details of morphology-dependent oxidation susceptibility are known on size scales comparable to typical solid-state domain features as well as domain connectivity and electronic communication (e.g., energy and charge transfer).

It is generally believed that oxygen weakly adsorbs to polymer segments that may be subsequently converted to a reactive complex or adduct with light.^[1,2,9] Despite the identities of specific precursors and mechanisms implicated in polymer degradation are often being hidden from view, the underlying roles of oxygen in determining long-term material stability are profoundly manifest.^[4,12,13] In fact, inadvertent oxygen doping is inevitable without extreme caution and environmental control although these measures are rarely taken in practice.^[14] Here, we aim to understand the nature of oxygen interactions with specific polymer structural forms and on size scales comparable to actual morphological features encountered in thin films. To avoid complications from ensemble averaging, we use a hybrid single molecule photoluminescence (PL) spectroscopy and imaging approach combined with self-assembly techniques to fabricate nanoscale polymer forms with similar morphological characteristics as bulk thin films. Namely, nanofibers of P3HT are prepared that possess both aggregated and nonaggregated domains although the physical dimensions limit the scale of heterogeneity under interrogation.

A major goal of this work is to go beyond existing views of oxygen doping to further understand the consequences of selective interactions and reactivity on the nanoscale. To this end, we utilize excitation intensity dependent imaging that affords control of oxygen doping selectivity and kinetics. Contributions from aggregated and nonaggregated regions are revealed by spectral filtering, which demonstrate a peculiar effect that, to the best of our knowledge, has not reported previously in P3HT. Namely, we observe some regions that gain in PL intensity while others, often on the same nanofiber, concomitantly lose intensity following exposures to high intensity light soaking ($>1 \text{ kW cm}^{-2}$). This “gainer–loser” effect exposes the susceptibility of distinct nanoscale domains to photoinduced oxygen doping and subsequent degradative reactions that are not apparent from ensemble-level studies. We further show that “loser” species are prone to excitation intensity-dependent PL saturation behavior, which is an attribute of aggregated polymer chains, whereas “gainer” species do not show significant saturation, similar to observations from solvated polymer chains.

2. Results and Discussion

2.1. Self-Assembly and Ensemble-Level Characterization of P3HT Nanofibers

Figure 1a shows electronic absorption spectra tracking the growth of P3HT nanofibers in anisole dispersions. Anisole is a poor solvent at room temperature where sparingly small fractions of P3HT dissolve. Upon heating mixtures above 70°C , a homogeneous solution is formed (orange trace). Immediately following removal of the heat source, new transitions appear

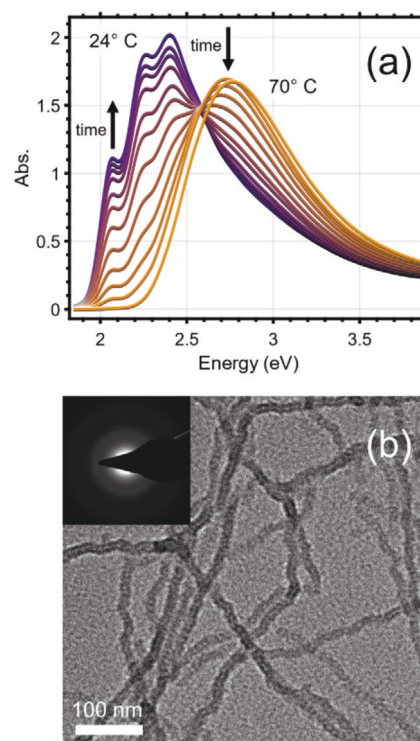


Figure 1. a) Electronic absorption spectra of P3HT nanofibers dispersed in anisole over a time period of ≈ 20 min. Samples were initially heated at 70°C to promote P3HT dissolution followed by removal of the heat source where formation of nanofibers occurs immediately upon cooling. b) TEM image and diffraction pattern (inset) of P3HT nanofibers.

on the red shoulder with a partially resolved vibronic progression ($\approx 1400 \text{ cm}^{-1}$). This new feature corresponds to π – π^* absorption transitions centered on aggregates, which grow significantly over time upon cooling (i.e., ≈ 20 min). Once ambient temperature is reached, all P3HT chains come out of solution in the form of nanofibers (purple trace). It is useful to point out that even with high dilution, these structures retain much of their form in solution rather than dissociating into smaller units. Subtraction of a portion of the cold chlorobenzene (CB)-solvated spectrum from the equilibrium anisole spectrum yields an estimate of the aggregate absorption (see the Supporting Information). **Figure 1b** displays a transmission electron microscopy (TEM) image of these structures that have characteristic widths on the order of ≈ 15 – 20 nm with lengths often exceeding several microns. Importantly, nanofiber morphologies resemble those of typical P3HT thin films where both aggregates and nonaggregated chains coexist along with their respective spectroscopic transitions. The upper size limit of aggregates in one dimension is clearly limited to the widths of the nanofibers although the presence of a substantial nonaggregated (amorphous) fraction makes typical domain sizes smaller. Moreover, anisole assembled nanofibers formed during uncontrolled cooling contain all components over the entire molecular weight distribution leading to greater disorder amongst aggregates.^[15] These nanoscale surrogates of bulk P3HT thin films now offer new opportunities to understand the effect of polymer conformation and packing on oxygen

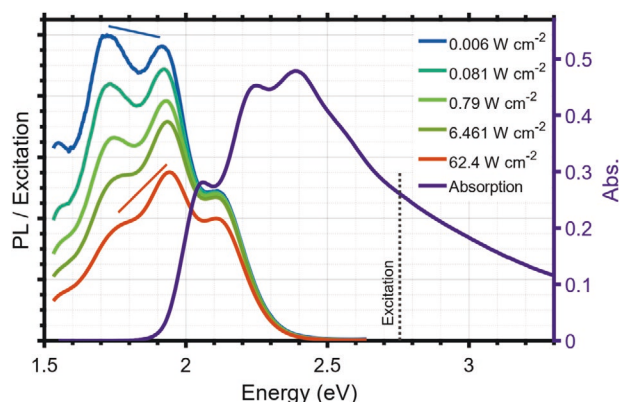


Figure 2. Excitation intensity dependent PL spectra of P3HT nanofibers in anisole. PL spectra were excited with pulsed 450 nm (2.77 eV) light. Low-energy emission is nonlinear in response to changing excitation intensities. The corresponding absorption spectrum is shown for comparison.

affinity, PL saturation, and photoinduced reactivity in addition to the effects of domain size and connectivity.

In order to first gain basic perspectives of structure-specific PL saturation behavior, we examined the excitation intensity dependent PL emission of P3HT nanofibers dispersed in anisole. These solution-phase samples were tested in ambient conditions and excited with a 450 nm (2.77 eV) pulsed laser. **Figure 2** depicts PL spectra of P3HT nanofibers at several different average excitation intensities along with a corresponding absorption spectrum of the original nanofiber dispersion. Dividing the detected spectrum by the excitation intensity allows comparison of signals of different magnitudes and highlights changes in efficiency: a strong dependence on excitation intensity is demonstrated.

Upon closer inspection of vibronic linewidths and known Stokes shifts observed in aggregates, the first resolved feature (≈ 2.1 eV) can be assigned as PL from nonaggregated P3HT

chains.^[16,17] It is important to note this feature shows far less intensity dependence than the corresponding lower energy features. Examination of the typical P3HT-film PL spectral region (< 2 eV) in **Figure 2**, lineshapes show characteristic features of aggregates with strong interchain electronic coupling (i.e., H-aggregate type) when excitation intensity is low (blue line).^[17] As excitation intensities increase from ≈ 6 mW cm $^{-2}$ up to ≈ 62 W cm $^{-2}$, relative intensities of the 1.95 and 1.72 eV peaks appear to decrease, but since solvated-type emission is present, the saturation of aggregate emission causes the proportions of each to change. It is also important to note that the ability of either emitting component to experience saturation depends on the rate of ground state depletion and excited state quencher yield and lifetime. In solvated P3HT chromophores, triplets may form although, since interchain chromophore electronic coupling is usually weak, this should not lead to appreciable saturation behavior. On the contrary, sufficiently aggregated P3HT samples are known to produce charges (polarons) that are highly effective singlet exciton quenchers. We speculate that combinations of this intrinsic mechanism with oxygen interactions are chiefly responsible for the large observed saturation behaviors in **Figure 2**. These results now provide a useful basis for correlating emission saturation (or lack thereof) with other qualities in the single molecule experiments (vide infra).

Additional insights into saturation behaviors may be obtained from PL decay dynamics at different emission energies and excitation intensities. Because the excitation source is the same as used for results in **Figure 2**, the results are directly comparable. **Figure 3** shows decay dynamics of P3HT nanofibers (anisole) corresponding to nonaggregated chains (550 nm, 2.25 eV) and aggregates (710 nm, 1.75 eV) (dashed and dotted lines). For comparison, similar decay dynamics were obtained from P3HT dissolved in dilute CB solution where aggregation contributions are negligible (solid lines). Virtually no change in either amplitude or time constants are observed in nonaggregated P3HT fractions (**Figure 3a**)

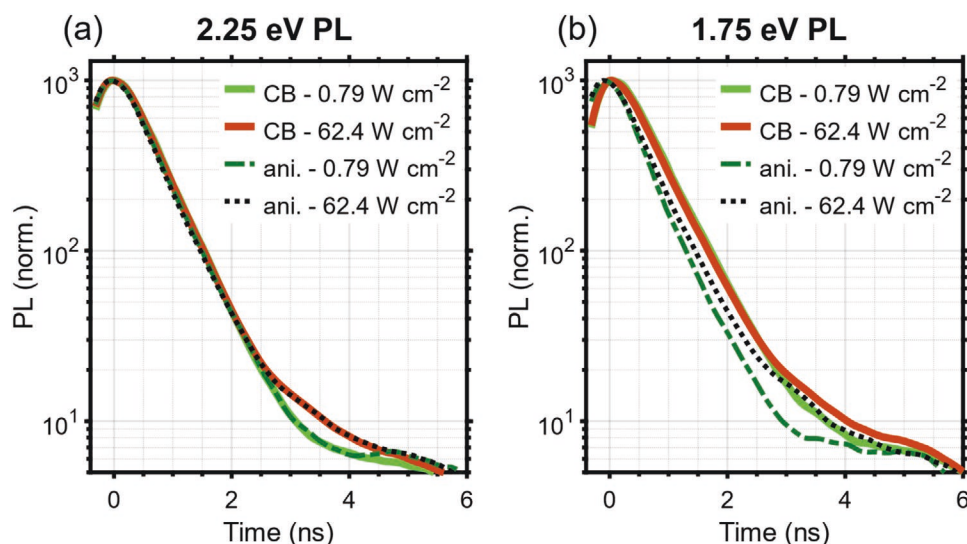


Figure 3. Time-resolved PL intensity decays of P3HT dissolved in dilute chlorobenzene (CB) solutions and anisole nanofiber dispersions measured at two different emission wavelengths. P3HT chains in CB solution show no evidence of aggregation.

for either conditions albeit a small increase in a longer time decay feature at higher excitation intensity. On the other hand, large excitation intensity dependent changes were observed in the aggregate emission component (Figure 3b) where larger excitation intensities led to a lengthening of the decay in nanofibers. From biexponential tail fitting of the anisole data, we find a dominant short time decay constant of ≈ 483 ps that was unaffected by excitation intensity along with a minority long time decay constant. Both the amplitude and time constant value changed with excitation intensity, e.g., 1.89 ns and $\approx 10\%$ of the fast component amplitude at the highest intensity compared to 8.53 ns and $\approx 1\%$ of the fast component amplitude at the lowest intensity. These results show that the excitation intensity dependence of aggregate-type emission in nanofibers is significant and multifaceted.

2.2. Resolving Preferential Oxygen Doping in Nanoscale Structural Domains Using Linear Excitation Intensity Saturation Schemes

Because anisole assembled P3HT nanofibers possess complex morphologies, it is necessary to go beyond the limits of ensemble averaging to understand oxygen doping effects on the size scales of individual domains. We use single molecule PL spectroscopic imaging by dispersing P3HT nanofibers into solid inert hosts (e.g., polystyrene). Linearly varying excitation intensity-dependent images were collected using different regimes where large changes in average power were introduced to accelerate light-driven processes. This approach exposes domain susceptibility to oxygen doping that can be directly spatially resolved. The basic experimental approach involves applying a sawtooth type waveform to a continuous wave, circularly polarized excitation source (488 nm, 2.54 eV) then recording PL emission synchronously with the excitation waveform. Because aggregated domains are expected to exhibit the greatest sensitivity to light-induced oxygen doping, we filtered the emission signal to select this component by placing a longpass filter (650 nm, 1.91 eV) in the emission path of the microscope imaging spectrometer. The specific approach involves an initial sequence of intensity ramping at low excitation intensity followed by a period of large intensities (e.g., $\approx 1000\times$) to “soak” these dilute solid dispersions of nanofibers then returned to similar values as used in the initial trajectory for the remainder of the experimental time window. **Figure 4a** shows a representative PL image (additional examples are included in the Supporting Information) obtained from the initial low power imaging, before any significant light-induced changes have taken place. Interestingly, some nanofibers and constituent regions displayed marked decreases in overall PL intensity counts while others showed large gains, which are indicated by purple and blue/green outlines, respectively. This effect was unexpected and has only been observed on one other occasion at the single molecule level^[18] but, never at the ensemble level.

It is only after the high intensity soak period, that differences in responses from distinct morphological features become more apparent. **Figure 4b** displays difference images over the same field-of-view as shown in **Figure 4a** depicting

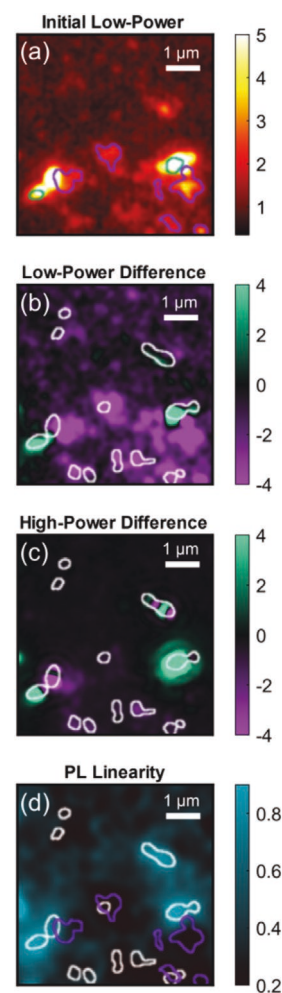


Figure 4. PL images generated by linearly ramping excitation intensities over three regimes (described in text). a) Average PL intensity imaging following an initial low intensity ramping period. Regions that gained or lost intensity are denoted by blue/green or purple boundaries, respectively. b) Difference image between PL intensities before and after a high intensity soaking period. White outlines depict spots and regions that bleached. c) Difference image during the high intensity soaking period constructed by z-scoring initial and final PL intensities. d) PL linearity image of all pixels generated by comparing the slopes of responses during ramping cycles on the low and high intensity limits.

changes between the low intensity trajectories before and after the high intensity soak. Outlines (white traces) are shown corresponding to features observed in the high intensity imagery and are provided as a guide for the eye. So-called “gainers” (green) and “losers” (violet) (i.e., fluorescence spots with larger and smaller PL intensities after the high intensity soak, respectively) are defined via their difference in standardized score from the image mean (which diminishes the effect of background).

Further insight into the susceptibility of these features as well as the overall bifurcation of P3HT nanofiber morphological components into “gainer” and “loser” categories can be found from comparing differences in integrated PL counts at the beginning and end of the high intensity soaking

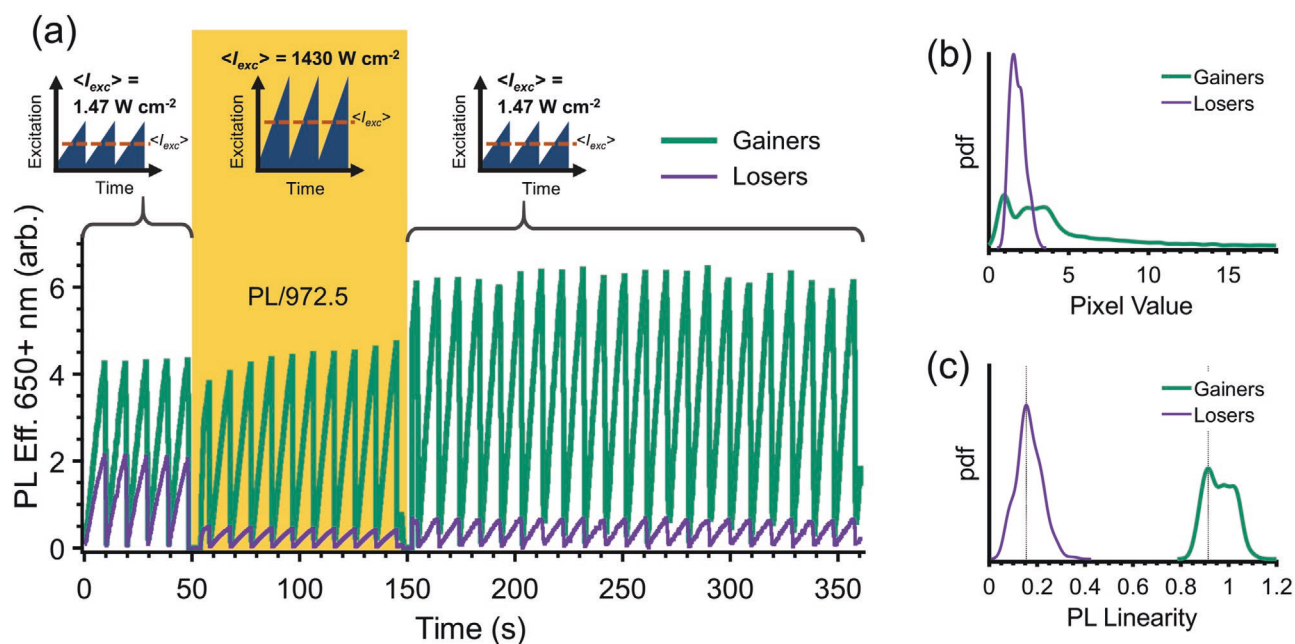


Figure 5. a) Excitation intensity dependent PL trajectories of subensemble classes of nanofibers showing intensity gains and losses, thresholded by four standard deviations from difference-image mean. Typical excitation intensities are displayed for each region with the high intensity soak highlighted in gold. In order to compare trends in saturation between low and high intensity regimes, it was necessary to scale PL intensities by the same factor as excitation intensities. b) Probability distribution function (pdf) of PL intensity displayed as the averaged, background subtracted pixel value for each subensemble during low-power imaging. c) Probability distribution function (pdf) representation of PL linearity for “gainer” and “loser” subensembles.

period. Figure 4c shows the high intensity difference image where often features within the same spot exhibit signatures of both emission types, i.e., “gainer–loser” regions within the same nanofiber. Despite that our spatial resolution is diffraction-limited (Rayleigh resolution limit $>260 \text{ nm}$), gainer–loser patterns often match textures observed in TEM images (Figure 1b). For example, straight sections in the nanofibers depicted in TEM images range from $\approx 25\text{--}150 \text{ nm}$, so it is possible that in some cases the high-power difference image (Figure 4c) resolves domains accurately, but in most cases it is more likely that some averaging is still taking place, since gainer–loser epicenters are often $120\text{--}240 \text{ nm}$ apart. We attribute these spacings to aggregated regions although the large variance in size and quality within P3HT nanofibers limits comparisons. Unfortunately, the nature of nanofiber processing does not afford the opportunity to achieve better uniformity in nanodomain sizes and composition. Nonetheless, this level of sensitivity in structure-dependent oxygen affinity cannot otherwise be obtained in ensemble-level samples and further demonstrates the utility of excitation intensity dependent PL imaging as a tool for resolving structure-specific oxygen doping on the nanoscale.

Because excitation intensity is linearly ramping during each period of the experiment, it is also possible to further correlate “gainer–loser” regions with their PL linearity. Interestingly, we find that “loser” regions tend to show saturation of PL emission much earlier than those of “gainers.” This effect can be understood by calculating the overall linearity during successive excitation intensity ramping cycles. Specifically, the slope of the emission response is fitted with a linear function over

an average of the first 5 ramps in the sequence (to alleviate signal-to-noise issues) and the lower-portion of the first complete ramp during the high intensity portion, and then taking their ratio. Figure 4d portrays responses from all spots where darker regions indicate substantial nonlinearity, which also corresponds to weaker PL intensity (the scale runs from 0.2, highly saturating, to 0.9, mostly linear).

Putative assignments of “gainer” and “loser” signatures can be inferred largely from previous reports of photophysical characteristics from distinct P3HT structural forms. For example, aggregation-induced quenching has been reported extensively at both ensemble and single molecule levels. It is reasonable to conjecture that weaker, more-saturable spots are indeed aggregated regions of nanofibers that also invariably show “loser” behavior. Likewise, all gainers show relatively linear responses over the entire excitation intensity range investigated. The apparent concomitant “gainer–loser” behavior also deserves comment, which can be traced to energy transfer between these distinct domains within the nanofiber. If favorable excitation energy funneling exists from the higher energy nonaggregated chains to aggregates, oxygen doping of the latter should increase the effect, at least until chain scission occurs, whereupon the funnel is destroyed and emission increases. Because of the large variability in domain sizes and purity within these nanofibers, we expect to find a nonuniform “gainer–loser” effect in solid dispersions, which is indeed the case.

The ability to spatially resolve structure-dependent oxygen interactions and doping in ultradilute P3HT nanofibers also permits sorting these behaviors into their respective classes to obtain clearer views of whether these effects persist on the

ensemble level. **Figure 5a** shows sorted “gainer” and “loser” subensembles demonstrating that these behaviors are in fact characteristic of structurally distinct P3HT morphological components and oxygen-specific interactions. It is also interesting to note that the gainer fraction exhibits increases in PL intensity while being exposed to high excitation intensities suggesting removal of quenchers probably from selective oxygen doping. **Figure 5b** also shows distributions of averaged PL intensities for each subensemble in terms of pixel values recorded on the CCD camera (background-subtracted).

Perhaps the more useful factor distinguishing “gainers” and “losers” is the effect of varying excitation intensity on PL emission linearity by sorting and averaging each behavior into their respective categories, which can be difficult to discern directly from only comparing single particles (i.e., **Figure 4d**). The linearity of PL responses in both subensembles was assessed using the same approach described earlier but then combining all single particles based on their behaviors. Averages from all sawtooth ramp excitation cycles were generated for each subensemble and plotted as a probability distribution function (pdf) in **Figure 5c**. Large differences in PL linearity are noted between the “gainer” and “loser” subensembles indicating the latter are much more prone to exhibit saturation. These trends further highlight the apparent stronger liability of the “loser” fraction with oxygen interactions. This effect is perhaps most apparent from examining the difference between the low excitation intensity images that bookend the high-intensity soak where some areas have experienced permanent photobleaching but were not strong enough in the original raw images to observe. These areas most likely correspond to aggregated domains based on ensemble-level trends (**Figure 2**) as well as known self-quenching characteristics. The latter effect has been reported most frequently in thin films, which is usually associated with facile polaron formation due to interpenetrating amorphous, nonaggregated chains creating a heterojunction-type interface.^[19] More pronounced PL self-quenching and saturation effects were demonstrated in single molecules of P3HT of varying molecular weight. Steiner et al. reported that

single P3HT chains efficiently funnel excitation energy to a low energy site, e.g., highly ordered aggregated segment in a triplet state, that functions as an energy acceptor for the entire chain.^[20] These authors showed greater PL intensity saturation as molecular weight increased, consistent with aggregates. In this study, samples are saturated with oxygen amplify photo-oxidation and saturation effects especially if efficient energy funneling from higher energy, nonaggregated domains is operative.

2.3. Unraveling the Mechanisms of the Gainer–Loser Effect: Ensemble and Molecular Perspectives

The mounting evidence of aggregates undergoing facile oxygen doping and PL saturation indicates a greater propensity for these structural forms to interact with oxygen molecules. Although ensemble level, excitation intensity dependent PL spectra showed clear saturation (**Figure 2**), these data cannot fully explain nanoscale effects where domain connectivity and electronic communication play vital roles in the appearance of “gainer–loser” behavior. Putatively, we propose that aggregated domains in P3HT nanofibers act as relative quenchers since these forms border amorphous regions and their destruction or saturation would lead to apparent increases in neighboring nonaggregated domains. Likewise, the usual excitation energy funneling mechanisms may also contribute where it is usually assumed the dominant energy transfer mechanism is a long-range Forster-type process. If energy transfer from nonaggregated to aggregated forms is significant, then we should expect a much larger “gainer–loser” effect due to removal of emissive aggregate traps.

In order to further confirm the role of aggregates in mediating oxygen doping as well as electronic communication between these and higher energy amorphous regions, we prepared identical nanofiber/PS samples that were subjected to an annealing treatment in low-oxygen conditions at high temperature then stored in different environments. This method

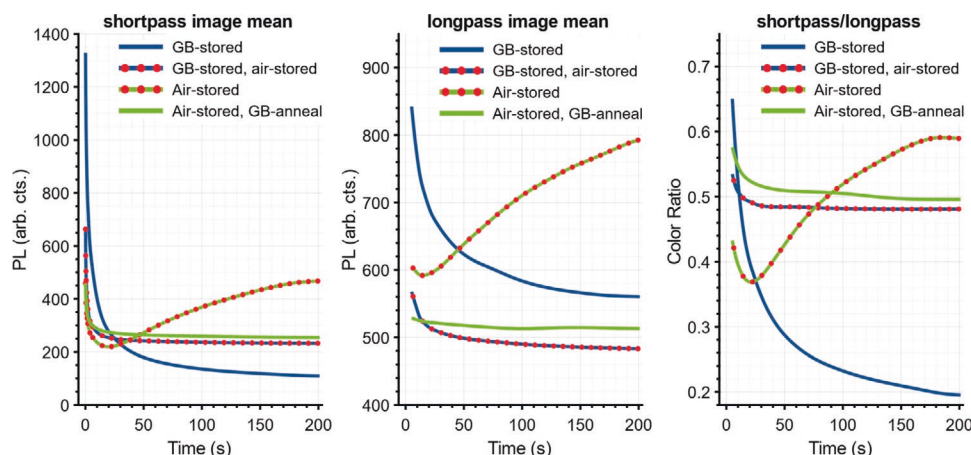


Figure 6. Time-dependent PL intensities averaged from many P3HT nanofiber responses from amorphous-dominant (shortpass filtered, 621 nm cutoff), aggregate-dominant (longpass filtered, 650 nm cutoff), and ratioed (shortpass/longpass) trends. Samples were either stored in a dry nitrogen circulating glovebox then taken out only for experiments (GB-stored), stored in the glovebox then kept in air for several weeks (GB-stored, air-stored), stored only in air (air-stored), or stored in air then thermally annealed in the glovebox.

allowed us to qualitatively assess the effect of varying oxygen content on different PL components. Energy filtered, time-dependent averaged PL intensities from these various samples are presented in **Figure 6** to facilitate comparison in responses. Samples kept in a dry nitrogen circulating glovebox showed drastic reductions in PL intensity leading to gradual photo-bleaching at longer times. This may be partially explained by local chain planarization and conformational relaxation from excitation leading to increased coupling (and quenched emission), since these samples were cooled by removal from the hot-plate, possibly leaving chains in nonrelaxed geometries. These effects were lessened somewhat when the glovebox-stored samples were placed in ambient air for at least two weeks although no evidence of particles showing distinct PL intensity gains was found for either aggregated or nonaggregated filtered emission. Only samples stored in air for long periods of time from the beginning displayed clear “gainer–loser” characteristics, which were especially prominent in longpass filtered images. However, the appearance of PL emission gains in the short-pass filtered data supports the hypothesis that the “gainer” phenomenon also contains significant contributions from disabled energy transfer to aggregates via photo-oxidation of sites with oxygen dopants.

By contrast, samples prepared and stored in air were thermally annealed in inert conditions and showed little change in PL intensity and color. These results offer strong evidence that aggregates preferentially trap oxygen and heating removes these adsorbed impurities in addition to generating more aggregates. By exposing the stability of multiphasic P3HT nanofibers with high excitation intensities, it is proposed that oxygen may either complex via a charge transfer type interaction that may subsequently form reactive species or deadsorb (dedope) in a manner similar to heating. The former is expected to dominate the “loser” effect where subsequent reactions effectively remove chromophores available for photoexcitation. Although it is difficult to quantitate branching ratios of oxygen-related photochemical outcomes, the clear bifurcation of “gainers” and “losers” highlights the interconnectedness and communication between distinct nanofiber domains.

2.3.1. Further Insights into the Molecular Origins of the “Gainer–Loser” Effect

Based on the trends thus far, we are able to reliably assign stronger PL saturation tendencies to P3HT aggregates due to their larger oxygen affinity and lower oxidation potentials. This attribute can most readily be traced to enhanced multidimensional electronic delocalization, which should stabilize interactions with oxygen. Along these lines, it has been shown that charge transfer complexes associated with oxygen are known to absorb at ≈ 2 eV similar to estimates predicted by the Rehm and Weller equation (from measured half-potentials).^[14,15] However, their low oscillator strengths complicate direct detection, especially in the case of P3HT which has overlapping and, much stronger, absorption transitions in this energy range.

Related oxygen-dependent effects akin to the “gainer–loser” phenomenon reported here is isolated P3HT nanofibers have also appeared in other studies of polymers at

both the ensemble and single molecule levels. For example, Botiz et al. showed vibrational evidence for excitation-induced chain planarization in MEH-PPV films and invoked it to explain their results with thin films showing slightly increased absorption ($\approx 4\%$ at peak) and increased emission ($\approx 20\%$ at peak) from soaking in white light in nitrogen conditions.^[21] Median PL lifetimes also become significantly shorter after light soaking, indicating an increase in the radiative rate, rather than a decrease in nonradiative pathways. However, in attempting to use these results to contextualize their own findings in drop-cast MEH-PPV films, Ho and White confirm the possibility of planarization but cannot replicate the change in lifetime that accompanied PL enhancement, thus they invoked interface effects to explain observed discrepancies.^[22] These authors proposed decreased interchain energy transfer from subtle changes in film morphology as the dominant cause for light-induced PL enhancement, but these studies are ultimately limited by averaging over conformational heterogeneity.

Martin et al. observed PL enhancement in single chains of MEH-PPV via selective excitation of the most delocalized chromophores in an ambient environment.^[18] Subsequent destruction via photo-oxidation was then invoked to explain observed PL enhancement and spectral blue-shifting. Further corroboration for oxidation-induced destruction of the excitation energy-funnel as a cause for PL enhancement was provided by ensemble level experiments on BDMO-PPV solutions by Deutsch and Park, which show that enhancement can outcompete chain scission for a portion of time in ambient conditions.^[23] These results are in good agreement with the “gainer–loser” effect reported here although direct spatial correlations and saturation effects were not provided previously.

Lastly, more efficient excitation energy transfer between P3HT forms leads to a larger “gainer–loser” effect. For example, apparent gains can be realized from PL intensity reductions from aggregate exciton quenching by holes, which is often reversible. However, much stronger enhancements are possible via selective photo-oxidation of those same delocalized chromophores. Complicating the elucidation of these processes are conformational rearrangements induced by excitation^[24] and oxygen-doping,^[25] which can reduce or increase PL intensities depending on the conjugated polymer and other conditions, as well as random chain scission via oxygen-related degradation.

3. Conclusions

In this work we use the preference for oxygen complexation with semicrystalline (delocalized) aggregate chromophores as a source of contrast to expose domain morphologies in nanofiber model systems of P3HT. PL enhancement is observed following high-intensity excitation soaking that we conclude is caused by destruction of low quantum yield energy funnels with latent oxygen doping. Furthermore, we show that facile saturation of PL emission is correlated with oxygen-doped aggregate domains, whereas amorphous domains are strongly emissive and exhibit near linear responses. The correlation of these

qualities is supported by ensemble-level characterization using many particles and creates new possibilities for less destructive detection of conformational domains using PL saturation as a metric.

4. Experimental Section

Samples: Regioregular poly(3-hexylthiophene-2,5-diyl) (Mn 54000–75000 Da), “electronic grade” was purchased from Sigma-Aldrich and used as-is. Nanofibers were formed by heating P3HT in anisole solution ($\approx 0.3 \times 10^{-6}$ M) in ambient conditions to >80 °C and then removed from the hotplate for quick cooling. Single molecule samples were made by spin-coating polystyrene (250 kDa, 2%w/w, 1k RPM) onto rigorously cleaned slides (including UV-ozonation), which resulted in a ≈ 50 nm buffer film, followed by anisole-nanofiber solution spin-coating. After analyte solution dispensation the polystyrene buffer layer was measured to be ≈ 23 nm or greater. Samples were stored in ambient conditions for ≈ 5 weeks before examination to ensure oxygen saturation. For the environmental control study, nanofiber dispersions were heated to 225 °C for 1 h in inert conditions, then cooled by removal from the hotplate. Later annealing was performed at 140 °C to lessen conformational changes. Additional sample preparation procedures and conditions are provided in the Supporting Information.

Ensemble Characterization Studies: A Shimadzu UV-2550 was used to perform absorption experiments, and an Edinburgh FLS 980 was used to perform emission experiments (including lifetimes) on solution-phase samples in 1 cm quartz cuvettes. Excitation was a 450 nm Edinburgh pulsed diode laser, with intensities controlled by usage of various discrete absorptive neutral density filters. TEM imaging was undertaken by drop-coating solution nanofiber dispersions on standard copper mesh grids with a 20 nm thick carbon support film (Ted Pella) and allowing all the solvent to evaporate. Images were acquired using a Technai G2 F20 S-Twin TMP TEM running at a standard accelerating voltage of 200 keV. Typical spot sizes were chosen to balance signal contrast while minimizing electron damage to the materials. Diffraction patterns were obtained by briefly converging the beam, which revealed two faint rings characteristic to highly polycrystalline samples. Two distinct *d*-spacings of 2.15 and 1.2 Å were obtained, which rule out higher order Bragg reflections of a single diffracting feature.

Single Molecule Spectroscopy: An epifluorescence microscope (Zeiss AxioScope 200) with a plan-apochromat 100 \times /1.40 NA oil immersion objective (Zeiss) was used to perform imaging experiments under flowing UHP nitrogen conditions. Samples were illuminated using a laser diode source (488 nm, phoxx) with circular polarization and typical intensities ranging from ≈ 1 –1000 W cm $^{-2}$. In order to avoid any distortions from the dichroic mirror, an additional, matching dichroic mirror (Semrock) was included before laser excitation light entered the microscope. PL emission was magnified by $\approx 3\times$ upon exiting the microscope then filtered by longpass edge filters to reject scattered excitation light. The PL emission was then imaged into an electron-multiplying CCD camera (Andor iXon 888). The temperature of the CCD chip was kept at -70 °C. The total image field-of-view was determined to be 4.7×10^{-6} cm 2 . Because P3HT nanofibers contain many chromophores, no additional measures were required to obtain high signal-to-noise ratios.

Saturation behaviors of P3HT nanofiber PL emission was carried out by directly modulating the laser diode via its analog input using a sawtooth-shaped excitation profile generated by an external function generator. The CCD camera was then triggered by the function generator to start the beginning of the sequence. Typical acquisition times for each frame were ≈ 0.3 s with ≈ 30 exposures per cycle. Because the period of the excitation ramping was relatively long (e.g., ≈ 10 s) no significant drift was observed between PL responses and the excitation waveform. Three different excitation regimes were used for each image saturation experiment; i) low intensity (≈ 1 W cm $^{-2}$), ii) high intensity (≈ 1 kW cm $^{-2}$), iii) low intensity (≈ 1 W cm $^{-2}$). The typical modulation range around each

excitation intensity regime was about a factor of 35. To prevent camera saturation in regime ii, a $\approx 50\%$ transmittance absorptive ND filter was placed in the emission pathway.

Supporting Information

Supporting Information is available from the Wiley Online Library or from the author.

Acknowledgements

J.K.G. acknowledges support from the National Science Foundation (CHE-1904943).

Conflict of Interest

The authors declare no conflict of interest.

Keywords

aggregates, emission saturation, oxygen doping

Received: March 12, 2020

Revised: April 3, 2020

Published online:

- [1] C.-K. Lu, H.-F. Meng, *Phys. Rev. B* **2007**, 75, 235206.
- [2] H.-H. Liao, C.-M. Yang, C.-C. Liu, S.-F. Horng, H.-F. Meng, J.-T. Shy, *J. Appl. Phys.* **2008**, 103, 104506.
- [3] a) N. Sai, K. Leung, J. Zádor, G. Henkelman, *Phys. Chem. Chem. Phys.* **2014**, 16, 8092; b) O. V. Kozlov, S. A. Zapunidi, *Synth. Met.* **2013**, 169, 48.
- [4] A. Sperlich, H. Kraus, C. Deibel, H. Blok, J. Schmidt, V. Dyakonov, *J. Phys. Chem. B* **2011**, 115, 13513.
- [5] M. Brinkmann, *J. Polym. Sci. B Polym. Phys.* **2011**, 49, 1218.
- [6] M. Manceau, A. Rivaton, J.-L. Gardette, S. Guillerez, N. Lemaître, *Polym. Degrad. Stab.* **2009**, 94, 898.
- [7] A. Aguirre, S. C. J. Meskers, R. A. J. Janssen, H. J. Egelhaaf, *Org. Electron.* **2011**, 12, 1657.
- [8] H. Hintz, H. J. Egelhaaf, L. Lüer, J. Hauch, H. Peisert, T. Chassé, *Chem. Mater.* **2011**, 23, 145.
- [9] Y. Aoyama, T. Yamanari, T. N. Murakami, T. Nagamori, K. Marumoto, H. Tachikawa, J. Mizukado, H. Suda, Y. Yoshida, *Polym. J.* **2014**, 47, 26.
- [10] T. J. Savenije, J. E. Kroeze, X. Yang, J. Loos, *Thin Solid Films* **2006**, 511–512, 2.
- [11] a) J. Gao, E. T. Niles, J. K. Grey, *J. Phys. Chem. Lett.* **2013**, 4, 2953; b) F. M. McFarland, L. Bonnette, E. A. Acres, S. Guo, *J. Mater. Chem.* **2017**, 5, 5764; c) J. Euvrard, A. Revaux, P.-A. Bayle, M. Bardet, D. Vuillaume, A. Kahn, *Org. Electron.* **2018**, 53, 135; d) I. E. Jacobs, E. W. Aasen, J. L. Oliveira, T. N. Fonseca, J. D. Roehling, J. Li, G. Zhang, M. P. Augustine, M. Mascal, A. J. Moule, *J. Mater. Chem. C* **2016**, 4, 3454.
- [12] R. D. Scurlock, B. Wang, P. R. Ogilby, J. R. Sheats, R. L. Clough, *J. Am. Chem. Soc.* **1995**, 117, 10194.
- [13] H. Ohta, H. Koizumi, *Polym. Bull.* **2017**, 74, 2319.
- [14] M. Nothhaft, S. Höhla, F. Jelezko, J. Pflaum, J. Wrachtrup, *Phys. State Solidi* **2012**, 249, 661.

- [15] a) T. P. Martin, A. J. Wise, E. Busby, J. Gao, J. D. Roehling, M. J. Ford, D. S. Larsen, A. J. Moulé, J. K. Grey, *J. Phys. Chem. B* **2013**, *117*, 4478;
b) J. D. Roehling, I. Arslan, A. J. Moulé, *J. Mater. Chem.* **2012**, *22*, 2498.
- [16] P. J. Brown, D. S. Thomas, A. Kohler, J. S. Wilson, J.-S. Kim, C. M. Ramsdale, H. Sirringhaus, R. H. Friend, *Phys. Rev. B* **2003**, *67*, 064203/1.
- [17] J. Clark, C. Silva, R. H. Friend, F. C. Spano, *Phys. Rev. Lett.* **2007**, *98*, 206406.
- [18] B. W. Martin, C. Melnychuk, L. J. Rothberg, *J. Photon. Energy* **2018**, *8*, 032219.
- [19] F. Paquin, G. Latini, M. Sakowicz, P.-L. Karsenti, L. Wang, D. Beljonne, N. Stingelin, C. Silva, *Phys. Rev. Lett.* **2011**, *106*, 197401.
- [20] F. Steiner, J. Vogelsang, J. M. Lupton, *Phys. Rev. Lett.* **2014**, *112*, 137402.
- [21] I. Botiz, P. Freyberg, C. Leordean, A.-M. Gabudean, S. Astilean, A. C.-M. Yang, N. Stingelin, *ACS Appl. Mater. Interfaces* **2014**, *6*, 4974.
- [22] X. L. Ho, J. D. White, *Chem. Phys. Lett.* **2019**, *735*, 136753.
- [23] M. J. Deutsch, H. Park, arXiv [physics.chem-ph] **2019**.
- [24] B. Morgan, M. D. Dadmun, *Soft Matter* **2017**, *13*, 2773.
- [25] P. Y. Yee, D. T. Scholes, B. J. Schwartz, S. H. Tolbert, *J. Phys. Chem. Lett.* **2019**, *10*, 4929.